

pubs.acs.org/chemneuro Research Article

On-Tissue Spatial Proteomics Integrating MALDI-MS Imaging with Shotgun Proteomics Reveals Soy Consumption-Induced Protein Changes in a Fragile X Syndrome Mouse Model

Min Ma, Qinying Yu, Daniel G. Delafield, Yusi Cui, Zihui Li, Miyang Li, Wenxin Wu, Xudong Shi, Pamela R. Westmark, Alejandra Gutierrez, Gui Ma, Ang Gao, Meng Xu, Wei Xu, Cara J. Westmark,* and Lingjun Li*



Cite This: ACS Chem. Neurosci. 2024, 15, 119–133



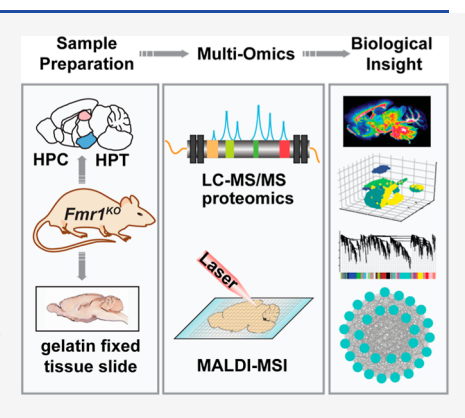
ACCESS

III Metrics & More

Article Recommendations

Supporting Information

ABSTRACT: Fragile X syndrome (FXS), the leading cause of inherited intellectual disability and autism, is caused by the transcriptional silencing of the FMR1 gene, which encodes the fragile X messenger ribonucleoprotein (FMRP). FMRP interacts with numerous brain mRNAs that are involved in synaptic plasticity and implicated in autism spectrum disorders. Our published studies indicate that single-source, soy-based diets are associated with increased seizures and autism. Thus, there is an acute need for an unbiased protein marker identification in FXS in response to soy consumption. Herein, we present a spatial proteomics approach integrating mass spectrometry imaging with label-free proteomics in the FXS mouse model to map the spatial distribution and quantify levels of proteins in the hippocampus and hypothalamus brain regions. In total, 1250 unique peptides were spatially resolved, demonstrating the diverse array of peptidomes present in the tissue slices and the broad coverage of the strategy. A group of proteins that are known to be involved in glycolysis, synaptic transmission, and



coexpression network analysis suggest a significant association between soy proteins and metabolic and synaptic processes in the *Fmr1*^{KO} brain. Ultimately, this spatial proteomics work represents a crucial step toward identifying potential candidate protein markers and novel therapeutic targets for FXS.

KEYWORDS: FXS, MALDI-IMS, label-free quantification, spatial proteomics, Fmr1, WGCNA

■ INTRODUCTION

Fragile X syndrome (FXS) is an X-linked neurodevelopmental disorder characterized by severe intellectual disability and other comorbidities including autism, seizures, anxiety, and attention-deficit/hyperactivity disorder (ADHD). FXS is caused by the deficiency or absence of fragile X messenger ribonucleoprotein (FMRP), an RNA-binding protein (RBP) with a prominent role in the regulation of a large number of mRNAs in the brain and periphery. Our prior research demonstrates that single-source, soy protein-based diets exacerbate seizures in mouse models of FXS, Alzheimer's disease, and Down syndrome, ² agreeing with numerous reports studying the effects of diet on CNS function.³ Soy-based diets contain high levels of plant estrogens (phytoestrogens, isoflavones), which can mimic or antagonize natural estrogen activity and affect neuronal excitability relevant to infant development.4 Given the prevalent use of soy-based infant formulas, we conducted retrospective medical record and survey analyses and found associations between the consumption of soy-based infant formula and an increased incidence of seizures, autism, gastrointestinal problems, and allergies in children with autism and/or FXS.5 However, the

lack of molecular biomarkers responsive to the consumption of single-source soy protein-based diets impedes the understanding of how soy protein affects FXS.

Matrix-assisted laser desorption/ionization (MALDI) mass spectrometry imaging (MSI) has become a powerful and successful tool for the detection and localization of a wide range of biomolecular species in recent years, including the imaging of lipids, 6 metabolites, 7 peptides, 8 proteins, 9 glycans, 10 neurotransmitters, 11 and drug compounds. 12 During a MALDI-MSI experiment, the laser beam moves across the surface of the matrix-covered tissue, which allows the desorption and ionization of biomolecules. 13 However, for complex tryptic digestion peptides, it is difficult to confirm the identification of an individual peptide solely on the basis of molecular mass.

Received: July 22, 2023 Revised: October 30, 2023 Accepted: November 30, 2023 Published: December 18, 2023





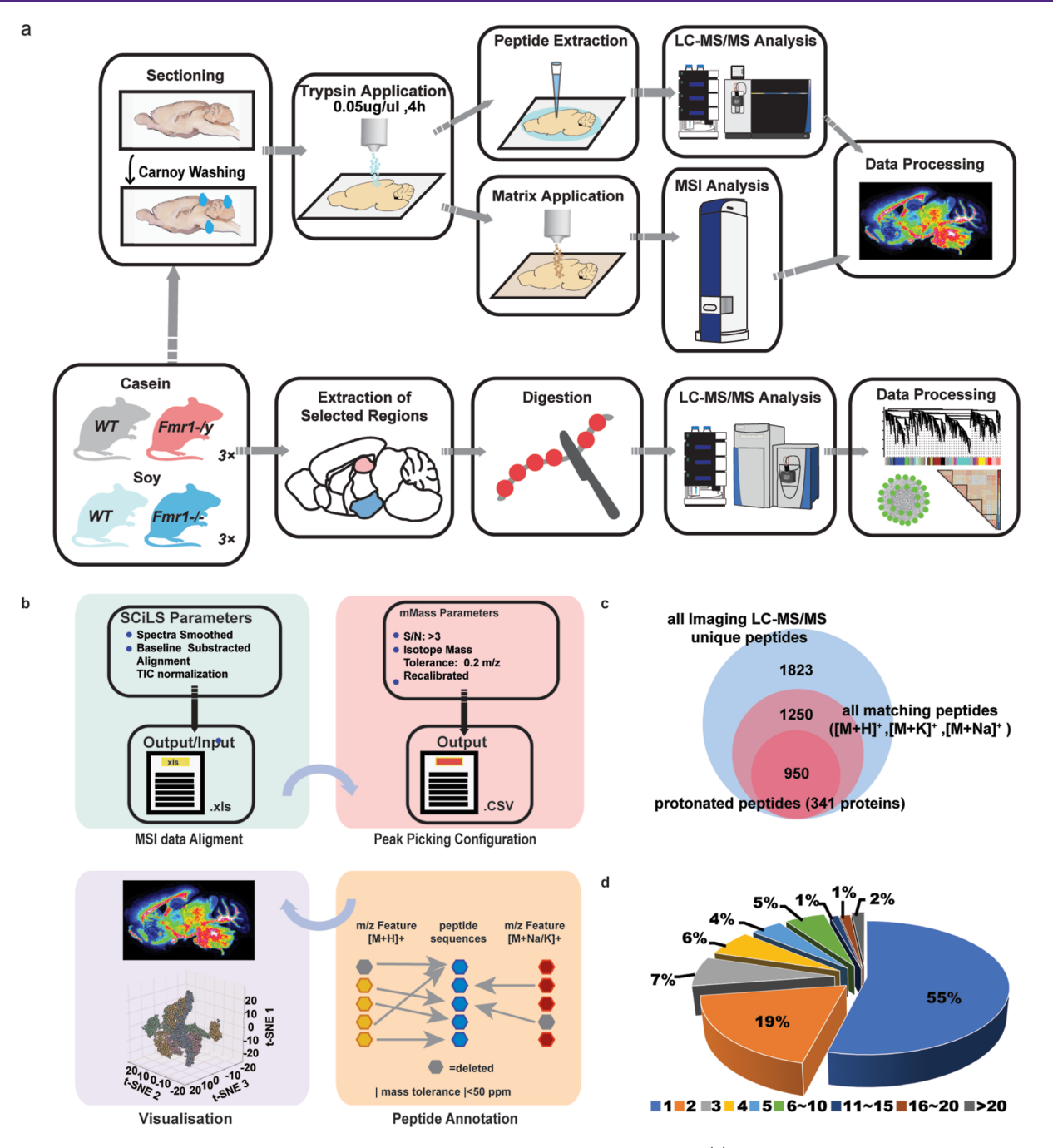
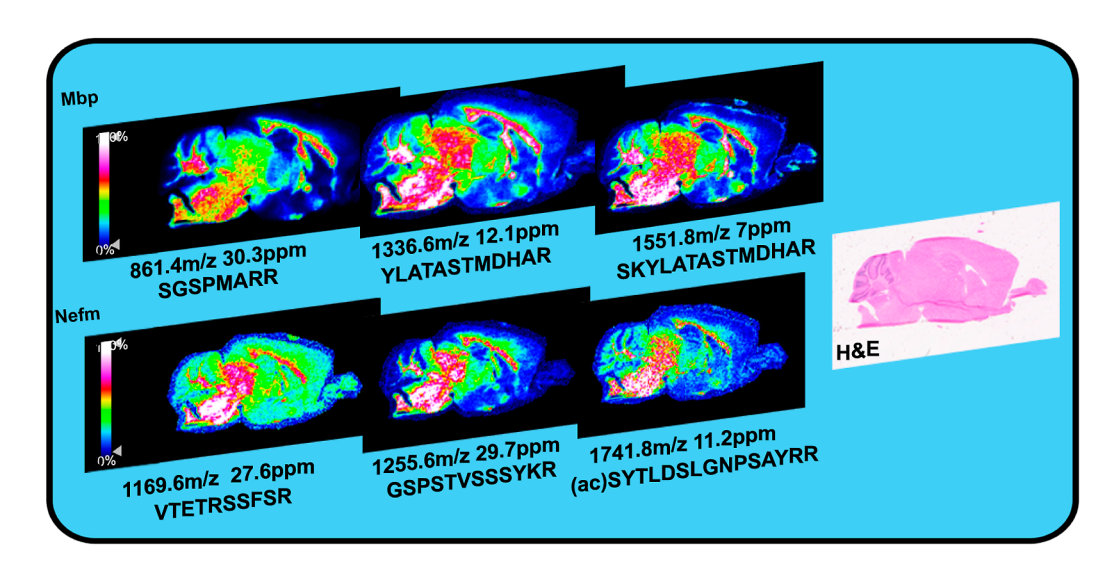


Figure 1. Multifaceted MS-based proteomic analysis of soy consumption in a FXS mouse model. (a) Schematic representation of the experimental strategy applied to resolve the spatial distribution of the proteome (upper panel) and quantitative landscape of the brain HPT and HPC proteomes (lower panel) of soy consumption from WT and KO mice. (b) Graphical illustration of automated annotation of spatial proteomic mass spectrometry imaging data. The raw files utilized for peak picking in mMass software are exported from SCiLS software. Parameters include imaging data preprocessing before exporting from SCiLS and S/N and isotopic mass tolerance when finding peaks via mMass (upper two panels); peptide annotation utilizes a peptide grouping strategy that deletes peptides that have larger mass errors or adduct peptides matched by one protonated peptide (lower middle panel); and visualization of spatially clustered peptide ion images, representing the summary protein spatial distribution across whole mouse brain tissues (lower panel). (c) Number of identified on-tissue LC-MS/MS unique peptides (class 1); all matching peptides, including protonated and adduct peptides (class 2); and unique matching protonated peptides (class 3) in MALDL-MSI. See Table S2 for more detailed information. (d) Pie chart depicting the percent distribution of multiple peptides assigned to one protein. The numbers of peptides for one protein are labeled with different colors from light blue (one peptide assigned to one protein) to dark gray (more than 20 peptides assigned to one protein).

To elucidate how the soy diet can affect FXS, we conducted a comprehensive proteomics analytical workflow integrating MALDI-MS imaging with shotgun proteomics to identify potential protein markers (Figure 1a). Our strategy reveals 1250 unique peptides, demonstrating the peptidome diversity

present in the tissue slices and the sensitivity of our technique. In addition, coexpression network analysis showed that the Fmr1^{KO} (KO) genotype and soy protein-based diet were significantly associated with metabolism and synapse modules via a comparison of proteins in a mitochondrial module with



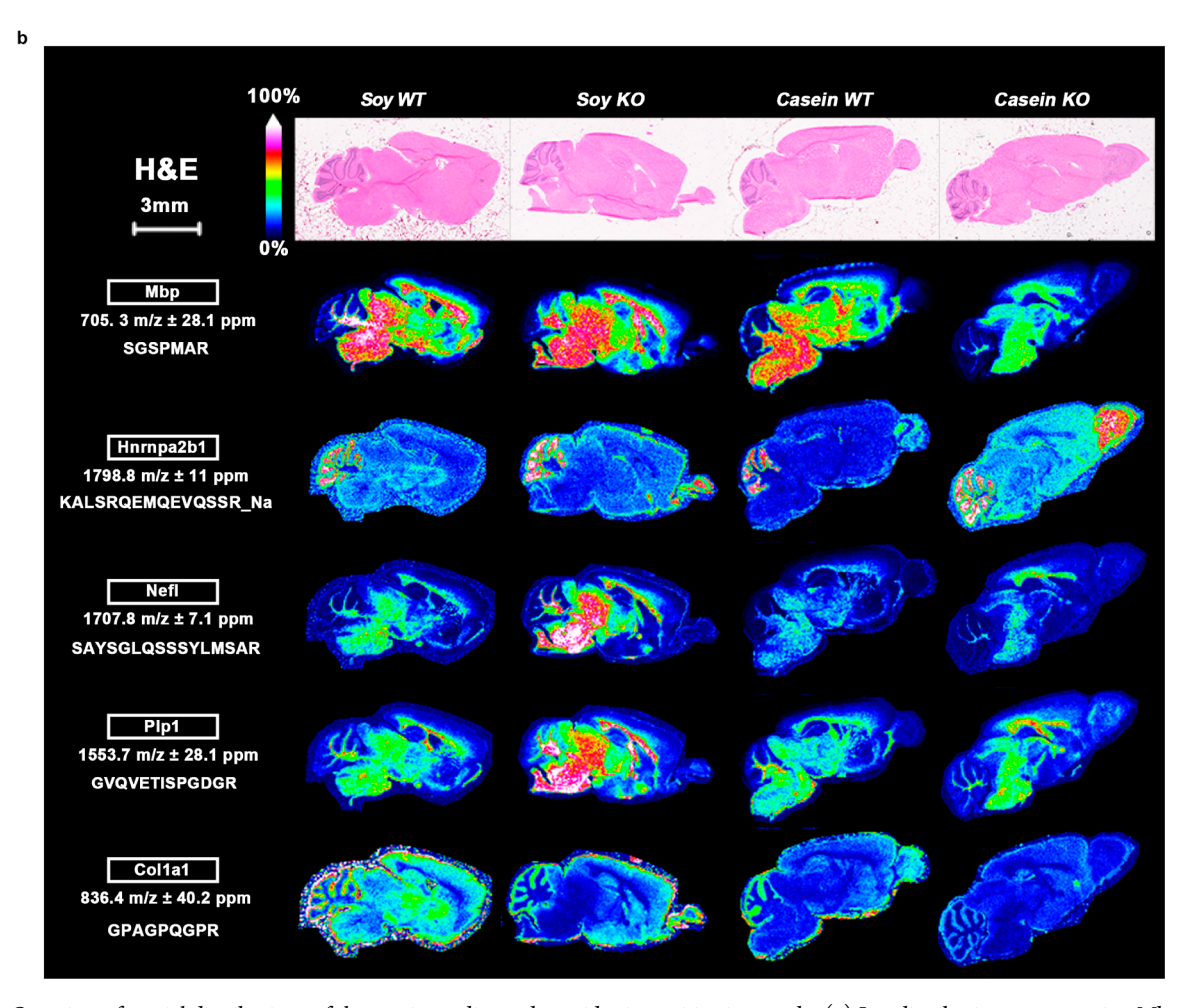


Figure 2. Overview of spatial distributions of the on-tissue-digested peptides in positive ion mode. (a) Ion distributions representing Mbp peptides (upper panel) and Nefm peptides (lower panel) obtained from Bruker rapifleX MALDI-TOF/TOF were assigned to peptides identified by ontissue tryptic digestion LC—MS/MS. Images were generated using SCiLS Lab. An image of a hematoxylin and eosin (H&E)-stained slice is shown to the right of the corresponding tissue slices. (b) Summed ion spatial distribution of different protonated peptides. Images were generated using SCiLS Lab. H&E-stained images are shown on top of the corresponding tissue slices.

glycolytic enzymes and the enzymes required for the tricarboxylic acid (TCA) cycle. Furthermore, our annotated peptide sequence from the MALDI MSI workflow was linked to global shotgun proteomics illustrating the complementarity

of MALDI MSI and LC-ESI MS/MS-based multiomics approaches. To our knowledge, this work is the first systematic application of spatial MALDI-MSI proteomics, combining spatial mapping and shotgun proteomics, to identify potential

soy-induced protein markers, which have important implications for the discovery and identification of therapeutic targets and biomarkers for FXS.

RESULTS

Construction of a Robust MS Imaging Pipeline for Mapping the Spatial Distribution of Tryptic-Digested Peptides in a Mouse Brain. Although significant progress has been made in MALDI-MSI in recent years, the analysis of proteins is still challenging due to lower signal intensity, low confidence annotations, and biased localization within the image. ¹⁴ Therefore, to determine the repertoire of the proteins in situ, the entire sample processing workflow requires careful optimization, from sample washing, enzyme concentration, and incubation conditions to the final MALDI mass spectrometry acquisition.

Two sample washing procedures were widely used in FFPE samples: a graded ethanol solution series⁹ and Carnoy's solution.¹⁵ Evaluating these two methods under the same humidity and tryptic digestion conditions, Carnoy's solution produced a significantly higher signal-to-noise (S/N) ratio based on the Wilcoxon signed-rank test compared to the original washing method among three biological replicates in our flash-frozen samples (Figure S1a).

After washing, tryptic peptides were extracted from two consecutive sections of each mouse brain tissue and separated and analyzed by LC-MS/MS. Usually, numerous candidates were retrieved for a given mass of interest in LC-MS/MS. An in-house script was used to provide automated postacquisition, matching of MALDI-MSI peaks, and tissue LC-MS/MS results. The entire matching workflow is divided into three parts, as illustrated in Figure 1b. First, regions of interest (ROIs) containing the entire area of the coronal section were selected in flexImaging. Then the raw files were imported to commercial software, Bruker's SCiLS Lab, for spectra smoothing and alignment¹⁶ and total ion count (TIC) normalization. For global preprocessing, the overall spectra for each of the analyzed sections obtained from SCiLS Lab were exported as comma-separated values (CSV) and read into the open-source software tool mMass. Mass spectral processing was performed using the following settings: (i) baseline subtraction, precision 25, and relative offset 5; (ii) peak picking, $S/N \ge 3$, and relative intensity $\ge 0.5\%$; (iii) deisotoping, isotope mass tolerance 0.2 m/z, and isotope intensity tolerance 50%; and (iv) recalibration based on the trypsin autolysis products and mass tolerance 50 ppm. The tissue-specific peaks were exported to Excel (Microsoft) to compare with on-tissue digestion LC-MS/MS results with a mass tolerance of 50 ppm. In tissue, the proportion of peptide signal from [Na]+ adducts may be higher relative to the [H]+ adducts depending on the tissue preparation procedure and natural salt concentrations in different tissues and tissue regions.¹⁷ However, since [H]⁺ adducts are still likely to be considerably more abundant than [Na]+ adducts, in this instance, priority was given to keeping the protonated peaks, if a peak could be matched to [Na]+ adducts and [K]+ adducts at the same time. For the case where multiprotonated peptides were matched, priority was given to peptides with the smallest mass error. Finally, the final peak list was imported into SCiLS Lab for imaging visualization.

Global Annotations for Peptide Identification in MALDI-MSI. To investigate the reproducibility of our peak picking and annotation strategy (Figure 1b), we tested four

study cohorts, including wild-type (WT) and KO littermate mice fed casein (C) or soy (S) protein-based diets. The peak list of each tissue section was corrected by subtracting all peaks detected in the gelatin tryptic digestion peptides (Table S1), which removed all m/z features originating from the gelatin embedding material. The resulting peak list was averaged among three biological replicates of each cohort (Figure S1b). All on-tissue-extracted unique proteolytic peptide sequences were matched with each biological deisotope peak list with a mass tolerance less than 50 ppm. The mean Pearson correlation value of relative peptide signals between the biological replicates of MALDI-MSI was excellent at 0.94, with a range of 0.772–0.993 (Figure S1c).

In total, nearly 69% of unique peptides from LC-MS/MS can be matched with the imaging peak list (Figure 1c and Table S2, sheet 1). Of note, 950 protonated peptides (Table S2, sheet 2), corresponding to 341 proteins, were assigned as MS² unique sequences (Figure 1c). Among those proteins, 55% had one peptide sequence assigned. Also, nearly 50% of the proteins include more than two tryptic peptides (Figure 1d), such as myelin basic protein (MBP) and neurofilament medium polypeptide (NEFM). For those proteins, we compared the peptide distribution within tissue sections (Figure 2a). The spatial distributions of the peptides were consistent with the parent proteins in the whole mouse brain, but distributions were found in different brain regions (Figure 2b). Heterogeneous nuclear ribonucleoprotein A2/B1 (Hnrnpa2b1), which is an RNA-binding protein and a nuclear reader of the m⁶A mark, ¹⁸ had higher expression in the cerebellum in all cohorts but was only enriched in the olfactory bulb region from the KO-C cohort (Figure 2b, third row). To further validate our strategy, the production of m/z 705.3 ([M + H]⁺) (Figure 2b, second row) and m/z 836. Four ([M + H]⁺) (Figure 2b, seventh row) were monitored in the TOF/ TOF imaging mode. Consecutive b/y ions were annotated in the MS/MS spectrum, and the peptide sequences were determined unambiguously (Figure S2). In addition, we also compared the 341 candidates to the curated database of mouse brain synaptic proteins (Genes to Cognition database, G2Cdb). 19 This identified an exceptionally strong overlap (45.5% of candidate proteins) with the postsynaptic proteome (PSP), which contains 1121 proteins (Figure S3a). We used the DAVID bioinformatics database (https://david.ncifcrf. gov/) to identify the top 40 pathways enriched (FDR < 0.05) in our targets (Table S2, sheet 3). Strikingly, the most significant overlaps included the biosynthesis of proteins involved in Alzheimer's/Huntington's disease, glycolysis, synaptic vesicle cycle/synapses, and signaling pathways (PI3L-Akt/HIF-1/mTOR), which suggest a direct role of diet in regulating the FXS proteome and cognitive and behavioral deficits. Finally, the tissue was successfully classified by performing a nonsupervised spatial segmentation analysis (Figure S3b). Taken together, this robust strategy not only has high reproducibility but also enables the exploration of distinct spatial distributions of protein markers. This information, combined with the annotated peptide sequences in the mouse brain, provides a powerful tool to identify potential biomarkers induced by soy protein consumption in KO mice.

Spatial Proteomics Reveals Potential Biomarkers in the Hypothalamus and Hippocampus. Feeding behavior is complex and modulated by various contextual factors and previous experiences.²⁰ The hypothalamus (HPT) plays key roles in appetite, food intake, whole-body energy homeostasis,

glucose metabolism, and body weight regulation.²¹ The hippocampus (HPC) controls fundamental learning and memory processes and is heavily influenced by feeding behavior.²² To identify altered expression of potential protein markers in HPT and HPC in response to the Fmr1 genotype, the four treatment cohorts were integrated into two groups and analyzed separately, i.e., the WT group (WT-C and WT-S) and the KO group (KO-C and KO-S). To further narrow down the list of promising targets, we screened all-matching peaks (Table S2, sheet 1) to ensure that the peaks were detected in at least two biological replicates in all cohorts, categorizing them as identified targets. Among the reproducibly detected peaks, 204 and 134 unique peptides were identified in HPC (Table S3, sheet 1) and HPT (Table S3, sheet 2), respectively, in the WT group (Table S3, sheet 3) and 308 and 236 unique peptides in HPC (Table S3, sheet 3) and HPT (Table S3, sheet 4), respectively, in the KO group. However, in comparing the two groups, some proteins were found to be specific to the KO group, including several FMRP candidate genes such as aconitate hydratase (Aco2), creatine kinase Btype (Ckb), and neural cell adhesion molecule 1 (Ncam1) (Table S3, sheet 5).

Given the complexity of comparing pixel-level intensity and the distribution of assigned m/z values across tissue sections, we employed t-distributed stochastic neighbor embedding (t-SNE) to help inform the underlying similarity and differences between the treatment groups. Full details can be found in the Supporting Information. Briefly, using adjacent, H&E-stained brain slices as a reference, HPT and HPC brain regions were outlined in SCiLS Lab, and the pixels lying within each region were normalized according to tissue-level total ion count and then exported for analysis. All HPT and HPC regions were concatenated into a two-dimensional array and coded by the treatment group (Figure S4a). The pixel-level intensity of each m/z value putatively assigned to a tryptic peptide was extracted and used to compile a three-dimensional training data set (Figure S4b,c). After iterative optimization to determine appropriate t-SNE parameters, data points were clustered in a three-dimensional space (Figure 3b). t-SNE clusters were manually rotated to better view each group; these plots may be viewed interactively, as described in the Supporting Information. In addition, except for the WT-S group, all of the other groups were clustered together. These data are consistent with our Pearson correlation coefficient results (Figure S1c). We reasoned that the WT-S group does not show a uniform distribution likely due to the larger variation of three biological replicates within the group.

In addition, a comparison of the protein-coding genes from the Darnell FMRP target data set²³ and the 1031 ASD genes from the SFARI autism database (https://gene.sfari.org/ database/human-gene/)²⁴ with our data set revealed varying degrees of overlap. A high degree of overlap was shown between our data and the Darnell FMRP target database-26 (11%) and 35 (18%) targets in the WT group and the KO group, respectively (Figure S3c), but only 16 and 15 targets were common between our data set and the SFARI database for the WT group and the KO group, respectively (Figure S3c). For example, MBP, whose mRNA is an FMRP binding target, has suppressed translation when FMRP binds to the 3' untranslated region.²⁵ However, how FMRP influences its translation during brain development and as a function of soyfeeding remains to be determined. Our imaging signal intensity showed that the level of MBP expression was upregulated in

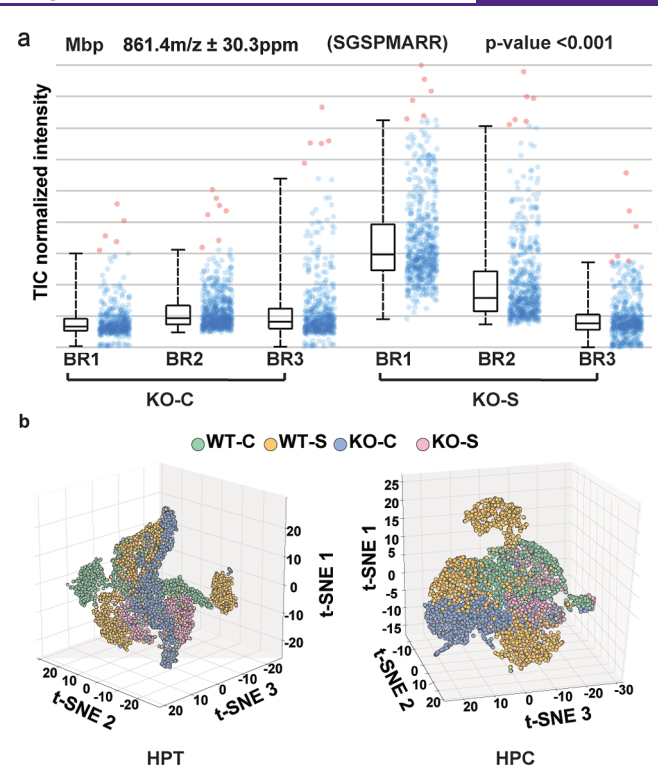


Figure 3. Annotated proteomes of FXS vs WT mouse brain tissues. (a) Normalized intensity of total ion signals of the Mbp unique peptide in three biological replicates (BRs) in HPT of the KO group in HPC. The boxplot points correspond to relative intensities of m/z 861.4-related peaks taken from each spectrum in all images acquired. The statistical tests were done via SCiLS Lab software using Student's t-test, and p-values were labeled. (b) The t-distributed stochastic neighbor embedding (t-SNE) visualization shows unsupervised annotated peak clustering, revealing four distinct cohorts in HPT (left panel) and HPC (right panel).

the KO-S cohort compared to that in the KO-C cohort in HPC (Figure 3a) and HPT (Figure S3d). This determination was based on the normalization of total ion current intensity from spectra in the respective HPC and HPT regions. The ROC plot showed that MBP can be used to discriminate treatment cohorts (Figure S3e). Thus, consumption of a single-source soy protein-based purified ingredient diet is associated with increased expression of MBP in both HPT and HPC in KO mice. The mechanism and biological significance of soy-induced dysregulation of MBP remain to be determined. There is reduced MBP and delayed myelination in KO mice.²⁶

Finally, we compiled a list of common targets from two published databases, and our imaging data set, which represents a core set of synaptic proteins encoded by autism-associated genes, bound at the mRNA level by FMRP and aberrantly expressed in response to a soy-based diet (Table S3, sheet 5). These proteins include sodium/potassium-transporting ATPase subunit beta-1 (Atp1b1), dihydropyrimidinase-related protein 1 (Crmp1), and rho guanine nucleotide exchange factor 2 (Arhgef2). Of note, the overlap among these data sets identifies potential biomarkers that are responsive to Fmr1 genotype and soy consumption and thus potentially involved in the development of autistic phenotypes.

Global Shotgun Proteomic Analysis. MALDI imaging mass spectrometry serves as a useful tool that enables simultaneous detection and spatial mapping of the distribution of putative peptide and protein signals; however, peptide

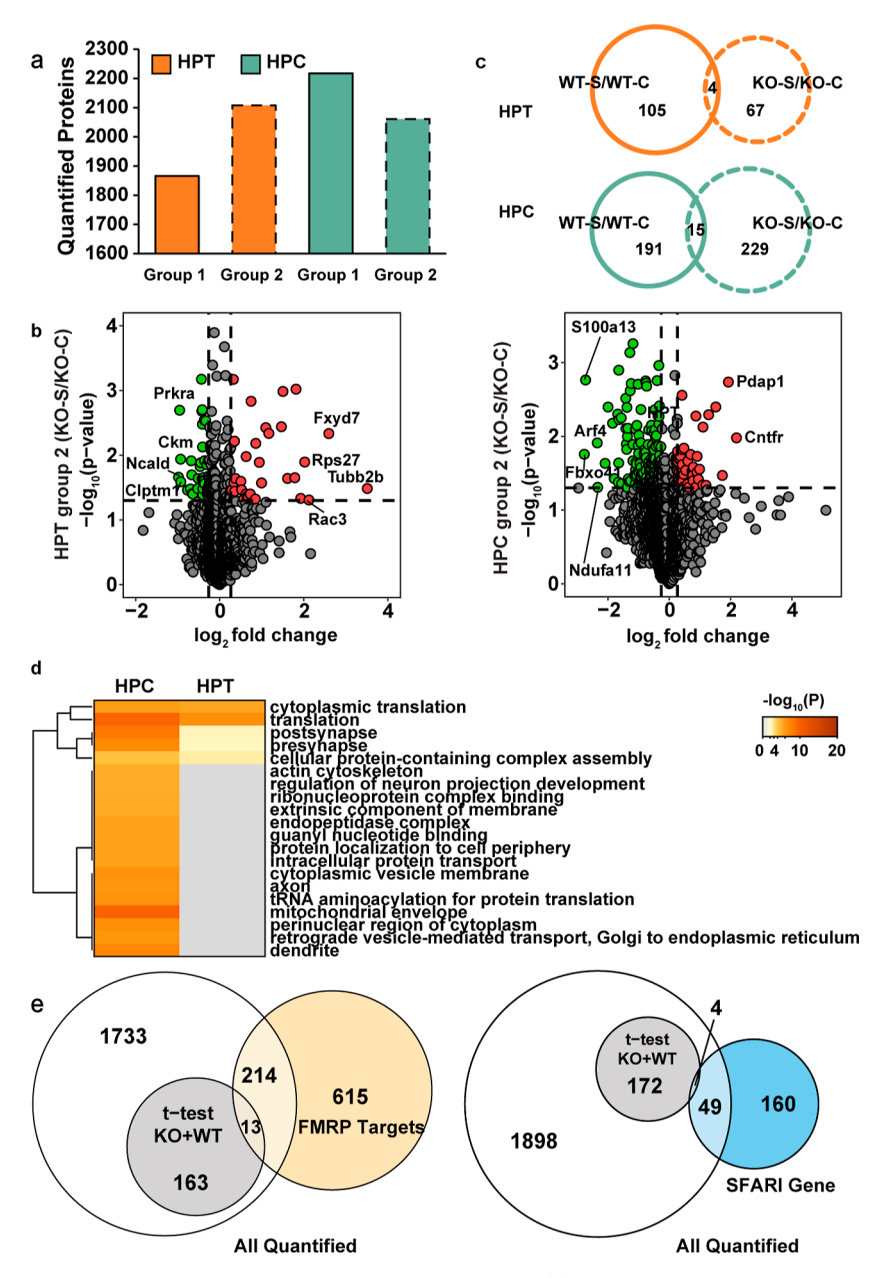


Figure 4. Global shotgun quantitative proteomic analyses of mouse HPT and HPC. (a) Number of proteins quantified using shotgun LC–MS/MS strategies in the WT group and the KO group in HPT and HPC, respectively. Bars with a solid line border represent the WT group, and bars with a dashed line border represent the KO group. (b) Volcano plots showed protein expression level changes between soy protein versus casein protein diets in the KO group for HPT (left panel) and HPC (right panel). Log₂ protein fold changes are plotted against the negative log₁₀ *p* values. Points above the nonaxial horizontal line represent significantly altered proteins (*p*-value < 0.05, Student's *t*-test). Significantly downregulated proteins are shown in green, and upregulated ones are shown in red (protein |fold change| > 1.2). (c) Significantly changed proteins using shotgun LC–MS/MS (*p*-value < 0.05, Student's *t*-test) from the WT group and the KO group were compared, and Venn diagrams demonstrate shared and unique proteins between the WT group and the KO group for HPT and HPC (solid line, WT group; dashed line, KO group). (d) Heatmaps generated using Metascape showing the significantly enriched (*p*-value < 0.01) biological processes, cellular components, molecular functions, and Kyoto Encyclopedia of Genes and Genomes (KEGG) pathways for the KO group in HPT and HPC. The most significant 20 terms are shown in the heatmap. Color coding indicates —log₁₀ (*p* values). Rows are clustered based on their profile similarity. (e) Comparison of the genes from all quantified proteins and significantly changed proteins (*p*-value < 0.05, Student's *t*-test) in HPT to gene entries from the FMRP target data set by Darnell et al. ²³ (yellow), as well as from the SFARI autism database (blue).

identification is still a major challenge due to low S/N ratios, low fragmentation efficiency for MALDI-produced singly charged precursor ions, and limited quantification capacity between different experimental cohorts. To address these issues, we conducted parallel analyses on tryptic digests of homogenized mouse HPT and HPC by LC–ESI MS/MS. Samples were collected from four cohorts (WT-C, WT-S,

KO-C, and KO-S) with 3 biological replicates and 3 technical replicates of each. Proteins were subjected to standard bottom-up proteomic workflows that involved tryptic digestion and label-free quantification to explore global protein abundance alterations and further correlate the findings with MALDI MS imaging results (Figure 1a). A total of 3521 and 3781 proteins (false discovery rate, FDR < 1%) were identified

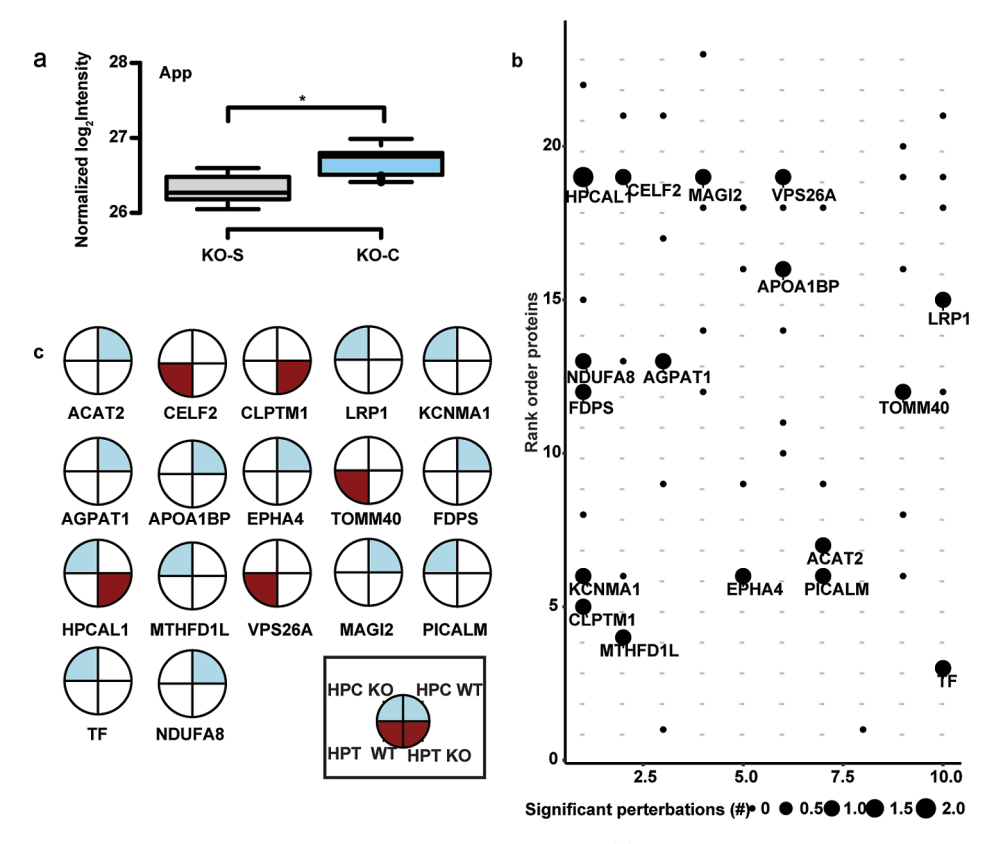


Figure 5. APP distribution and altered protein abundance of genes linked to LOAD. (a) Box plots of expression levels of APP protein in FXS mice in HPT as a function of diet. *p*-value < 0.05 was determined by Student's *t*-test. (b) Significant (*p*-value < 0.05) protein changes mapped to 17 genes previously linked to LOAD (dashed, not quantified). (c) Protein abundance with significant changes plotted with brain region and genotype information. Blue, HPC; red, HPT.

across the 4 cohorts in HPT and HPC, respectively (Table S4, sheet 1 and Table S5, sheet 1). Proteins were subjected to a binary comparison between a soy protein versus a casein protein diet in the WT group and the KO group. Those identified in at least two biological replicates in each cohort were considered quantifiable and resulted in 1866 (WT group; Table S4, sheet 2) and 2108 (KO group; Table S4, sheet 3) quantified proteins in HPT and 2217 (WT group; Table S5, sheet 2) and 2061 (KO group; Table S5, sheet 3) quantified proteins in HPC (FDR < 1%, Figure 4a).

To determine proteins with significant alterations, all quantified proteins were subjected to Student's t-test, and representative results for the KO group in HPT and HPC are visualized in volcano plots and demonstrated in Figure 4b (Table S4, sheet 3 and Table S5, sheet 3). Points above the nonaxial horizontal lines represent proteins with significant alterations (|fold change| > 1.2, p-value < 0.05). To explore protein alterations associated with the FXS model in HPT and HPC, we further demonstrated specific proteins, which significantly changed only in the WT group or KO group or showed dramatic fold changes between the two cohorts (Figure 4c; Table S6 for HPT and Table S7 for HPC). To better discern differential regulations in HPT and HPC, we generated heatmaps showing multigroup Gene Ontology (GO) analyses in Metascape.²⁷ The 20 most significantly enriched biological processes, cellular components, molecular functions, and KEGG pathways are shown in Figure 4d, where the color-coding indicates the p-values of a certain term in different groups. Since more proteins were dramatically changed in HPC, most GO terms involved in HPT were

also enriched in HPC, clearly showing disparities between the two regions when exposed to soy consumption. In HPC, proteins are mostly enriched in the axon, dendrite, and mitochondrial envelope and are associated with GO terms such as guanyl nucleotide binding and regulation of neuron projection development. These alterations may reflect differential responses in varied brain regions as a function of the soy diet and aid in the discovery of potential nutritional biomarkers. Serving as the baseline comparison, we also explored the effects of soy- and casein-based diets in the WT group (Figure S5a-c).

Furthermore, proteins that exhibited significant alterations via Student's *t*-test were combined and compared with the Darnell data set as shown in the Venn diagrams for HPT (Figure 4e). We found 227 targets in common, of which 13 were significantly changed after soy consumption (Table S8, sheet 1). We also compared our data set with the SFARI autism database, which listed 196 genes associated with autism spectrum disorders, of which 16 were significantly altered after soy consumption (Table S8, sheet 1). Parallel comparisons between HPC proteins and two data sets are shown in Figure S6b (Table S8, sheet 2).

Of particular interest to our laboratory is the role of amyloid- β precursor protein (APP) in FXS. APP is processed by β - and γ -secretases to generate β -amyloid, the predominant peptide found in senile plaques in Alzheimer's disease. APP mRNA is a well-validated target of FMRP. Here, we observed upregulation of APP levels in the KO group compared to that in the WT group in HPT with both diets (Table S4, sheet 4 and sheet 5), in agreement with our

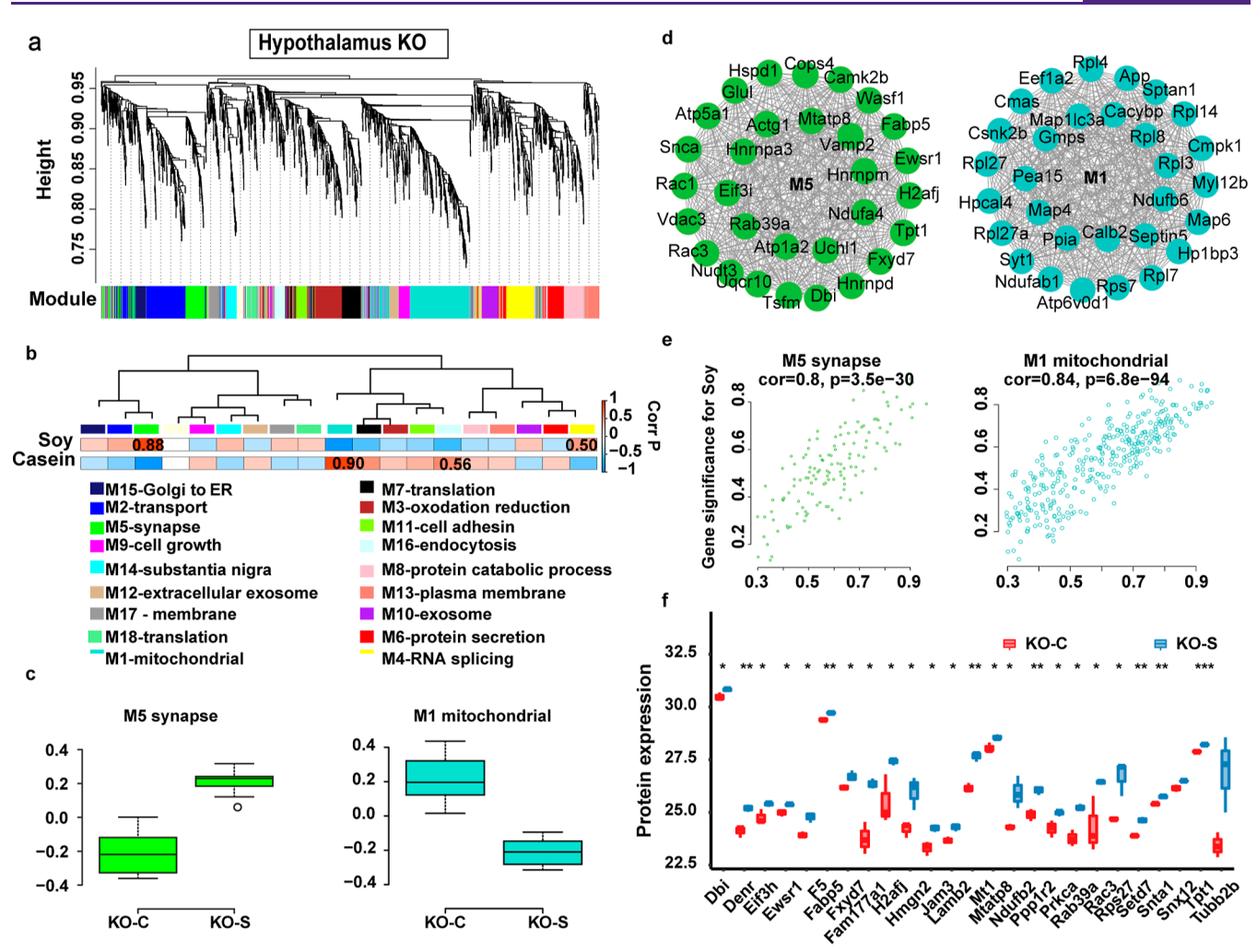


Figure 6. Consensus protein coexpression network analysis of FXS. (a) Protein clustering trees generated in the KO group for HPT. Each ME is in nongray. (b) Protein correlation network consisting of 19 protein modules was generated from 2108 proteins in the KO group for HPT. Module eigenproteins, which represent the first principal component of the protein expression within each module, were correlated with diet traits. The strength of a positive (red) or a negative (blue) correlation is shown by a two-color heat map, with p values provided for all correlations with p < 0.05. Modules that showed a significant correlation with diet traits are labeled with a correlation value. GO analysis of the proteins within each module clearly identified the biological functions, processes, and components associated with the module (bottom). (c) A synthetic eigenprotein was created to network two modules. Summary eigenprotein expression value from casein- or soy-diet for M5 synapse (left) and M1 mitochondrial (right) that had significant correlation to diet traits. Whiskers extend to data points that are less than 1.5* interquartile range away from the 1st and 3rd quartiles, respectively. The horizontal line shows the median. (d) Network of the top 50 hub proteins in the M5 synapse (left) and M1 mitochondrial (right) in the KO group for HPT. (e) Visualization of GS vs MM and gene expression levels of significant modules. The scatterplot represents the GS and MM of each module that shows a significant correlation (p < 0.05), implying that the module tends to be associated with the soy diet. Module membership versus gene significance for the M5 synapse (left) and the M1 mitochondrial (right). (f) Significantly changed proteins involved in M1 mitochondrial. Box plots represent the median and the 25th and 75th percentiles, and whiskers represent measurements to the 5th and 95th percentiles. Differences in protein levels were assessed by Student's t-test (*p-value < 0.05, **p-value < 0.001, and ***p-value < 0.0001).

published data of elevated APP in the KO. We also observe a significant decrease in APP levels in HPT in the Fmr1^{KO} group in response to the soy diet (Figure 5a, KO–C versus KO–S). The mechanisms underlying the translation and processing of APP in response to soy consumption remain to be elucidated. To further correlate significantly altered proteins with genes predisposed for AD, we examined the overlap between genes linked to late-onset AD (LOAD) and proteins with altered abundance in the KO mouse brain. We identified 17 significantly altered proteins genetically linked to LOAD (Figure 5b). Only hippocalcin-like protein 1 (HPCAL1), which serves as a sensor of Ca²⁺ and enhances the Wnt pathway, was altered in two groups, and the remaining

targets were differentially expressed in one group (Figure 5c). These findings indicate that some of the genes linked to LOAD also have altered protein products in the KO mouse brain, further highlighting the intriguing connection between AD and FXS that warrants future mechanistic investigation.

Integrated Bioinformatic Analysis to Decipher Molecular Function by Incorporating WGCNA. This study adopted the weighted correlation network analysis (WGCNA) algorithm to better analyze and predict the molecular function of soy on protein expression in FXS. We were able to generate consensus networks across genotypes and phenotypes for both the HPT and HPC data sets. A total of 2108 proteins were screened for the WGCNA analysis in the KO group HPT.

After normalization, no outlier samples were eliminated. The power of $\beta = 6$ (scale-free $R^2 = 0.9$) was selected as the softthresholding parameter to ensure a scale-free network (Figure 6a). A total of 19 modules (M) with similar expression patterns were identified via the average linkage hierarchical clustering (Figure 6b). GO analysis of the protein module members demonstrated diverse ontology for all 19 modules regarding biological functions, processes, and components (Figure S6). We then correlated module eigenprotein (ME) to different soy- or casein-based diet cohorts to assess whether a given coexpression module was related to diet (Figure 6b). The module and diet traits were considered statistically significant when p < 0.05. We observed two modules that exhibited the strongest association with diet traits. The M5 (synapse) module, which consisted of 130 proteins, showed the strongest trait correlations with the soy-based diet (corr p = 0.88), while the M1 (mitochondrial) module, which contained 348 proteins, exhibited the best correlation with the casein-based diet (corr p = 0.90). By decomposing our MEs into individual diets, we assessed the relationship of MEs to different diets and measured the module eigenprotein values (summary expression profile) by case status (Figure 6c). We found that M1 and M5 (synapse) have statistically significant differences (Z statistic and corresponding meta-analysis p-value < 0.05) between the soy and casein cohorts. M5 (synapse) exhibited increased protein levels, while M1 (mitochondrial) showed decreased protein levels in the soy group. In addition, we performed network analysis based on the continuous measure of membership and connectivity based on WGCNA to determine the top 50 hub proteins in M5 and M1 and visualized them using Cytoscape (https://cytoscape.org/) (Figure 6d). To evaluate the significance of modules, gene significance (GS) was calculated as the correlation between genes and each trait. The module membership (MM) was defined as the association between gene expression profiles and the module's own genes. Subsequently, genes within cor. Gene MM > 0.8 and cor.Gene GS > 0.8 are considered key proteins. Both M1 and M5 represented the highest positive correlation with single-soy consumption (Figure 6e). Finally, 25 significantly changed proteins were found in the M5 module. Ras-related protein Rab-39A (Rab39a), FXYD domaincontaining ion transport regulator 7 (Fxyd7), and Fatty-acidbinding protein 5 (Fabp5) were upregulated in the KO-S cohort compared to that in KO-C (Figure 6f). Differences in protein levels were assessed by Student's t-test. The WT group, as a control group, was also analyzed by WGCNA; more details are shown in Figure S7a-d and GO analysis of the module members is shown in Figure S8.

To assess whether the network was similar in other brain regions, we conducted the coexpression network analysis for the HPC KO group (Figure S9a-c). A total of 2061 proteins were used to generate six protein coexpression modules, which ranged in size from 662 proteins (M1) to 69 proteins (M6). The GO analysis of the proteins within each module clearly identified the biological processes associated with the module. Other GO analyses of cellular components and molecular function terms are shown in Figure S10. We observed three modules that were significantly correlated with diet phenotype (see Figure S9a, right panel): modules M1 mitochondrial, M2 synapse, and M3 metabolism. The M3 metabolism module showed the strongest single-soy diet trait correlation (corr p = 0.90), but the M1 and M2 modules showed the strongest negative correlation of soy traits (M1 corr p = 0.90 and M2

corr p = 0.90). Noticeably, M1 and M2 modules decreased in the KO-S cohort compared to that in the KO-C cohort, but the M3 module showed the opposite trend (Figure S9b). In addition, we performed network analysis based on the continuous measure of membership and connectivity based on WGCNA to determine the top 50 hub proteins in M1, M2, and M3 and visualized them using Cytoscape (Figure S9c). The WT group as a control group was also analyzed by WGCNA with details shown in Figure S11a,b and GO analysis of the module members in Figure S12.

Noticeably, the module function of mitochondrion-related module eigenprotein values by case status showed similar differences between case cohorts in HPT and HPC. Recent work by Licznerski et al. suggests that loss of FMRP causes a mitochondrial inner membrane proton leak that prevents synaptic maturation.³¹ To explore the effect of soy consumption and the *Fmr1* genotype on mitochondrial regulation, we integrated MALDI MSI data with proteomics data to demonstrate the spatial distribution of proteins and provide a resource for interrogating the biological basis of mitochondrial dysregulation (MD).

Spatially Resolved Proteins Correlated with Shotgun Proteomic Analysis. Even though MALDI-MSI excels in providing spatially resolved molecular information within tissue sections, it typically provides limited molecular identification and quantification. Hence, to enhance confidence in the quantification of our data, we conducted a systematic comparative analysis between the MALDI-MSI and LC-MS/MS data sets. After comparing the peptide list from MALDI MSI experiments to all quantified peptides revealed by LC-MS/MS in the WT group and the KO group in the HPT and the HPC, an average of 85.6% of the imaging proteins could be quantified in proteomics data (Figure S13a). Among the common proteins, 15 proteins associated with glycolysis and the TCA cycle (Figure S13b) were involved in spatially resolved proteomics.

The glycolytic enzyme enolase 1 (ENO1), whose level was upregulated 1.2-fold in the KO-S HPC proteomics data compared to that in KO-C, showed the same dysregulation by MALDI imaging (Figure 7a). We subsequently assessed ENO1 protein expression in mouse brains to further investigate the expression of ENO1 regulated by soy food intake via IHC. Immunohistochemical examination showed clear staining of ENO1 in HPC CA1, CA3, dentate gyrus (DG), and hilus (H) regions (Figure S14a). The level of ENO1 was also increased in HPC CA1, CA3, DG, and H in the KO-S cohort compared to that in the KO-C cohort (Figure 7b,c). However, the WT group showed no statistical difference in the MALDI-MSI data set (Figure S14b), and IHC staining further confirmed the MALDI-MSI results (Figure S14c,d). However, GAPDH, a key glycolytic enzyme that is associated with an elevated risk of developing AD, 32 was only identified in the imaging data pool and was upregulated in the soy cohorts compared to the casein cohorts across brain regions in KO in both HPT and HPC (Figure S15a,b). Thus, consumption of a single-source soy protein-based diet is associated with mitochondrial dysregulation, although the mechanism and biological significance of related, elevated protein levels for FXS remain to be determined. In addition, other well-known FMRP targets resolved in spatial proteomics and shotgun proteomics that were significantly changed included stathmin (STMN1), glucose-6-phosphate isomerase (GPI), microtubule-associated protein tau (MAPT), and other candidates (Table S8, sheet 3).

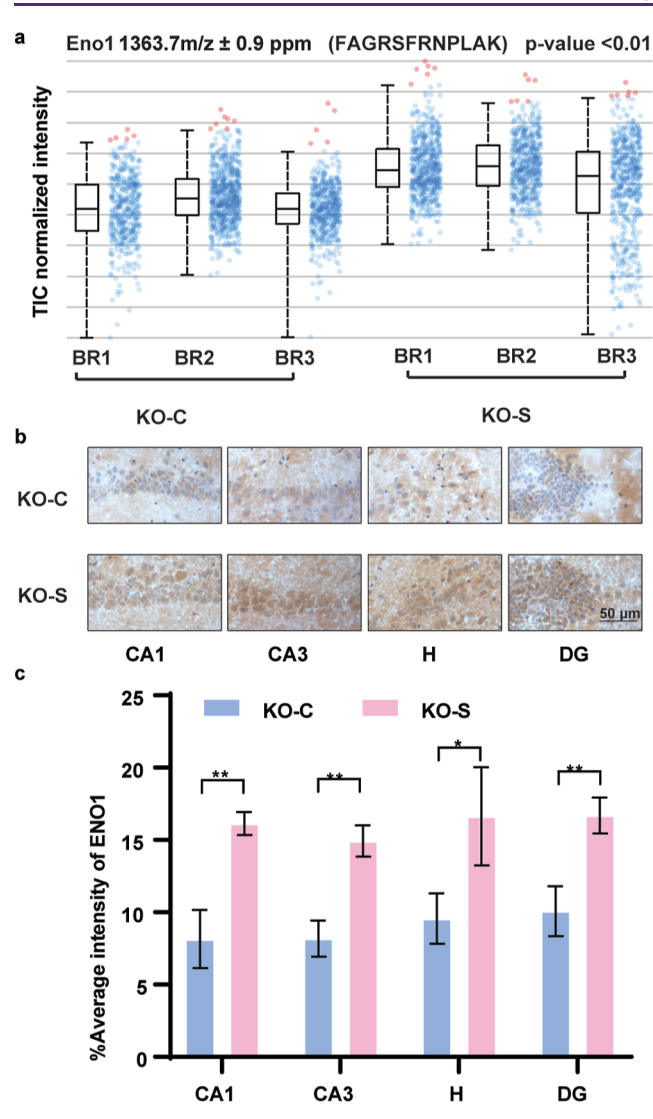


Figure 7. ENO1 was upregulated in the KO soy-food intake cohort. (a) Normalized intensity of total ion signals of ENO1 in three biological replicates in HPC of the KO group. The boxplot points correspond to the relative intensities of m/z 1363.7-related peaks taken from each spectrum in all images acquired. (b) Example of IHC images showing ENO1 protein in CA1, CA3, H, and DG of the KO mouse brain. Images of 'The KO group of casein (KO–C, upper panel) and soy (KO–S, lower panel) cohorts'. Scale bar, 50 μ m. (c) Statistical analysis of the IHC image intensity. Three biological replicates of each cohort (KO–S and KO–C) were used. The data was analyzed for each cohort. p-value determined by a two-paired Student's t-test (*p < 0.05 and **p < 0.01). Area average intensity is shown in mean \pm SD.

Of importance, metabotropic glutamate receptor 5 (mGluR5) was significantly downregulated in the KO group in HPC in response to the soy diet (see Figure S15c, p-value < 0.05, \log_2 (fold change) = -1.5) but notably not in the WT group. Multiple studies have shown that altered mGluR5 signaling plays an important role in FXS pathophysiology. These findings further highlight the potential impact of the soy diet on neural plasticity and behavioral responses. Taken together, all quantified proteins are highly correlated with the synapse and mitochondrial energy module functions.

DISCUSSION

Consumption of single-source, soy-based diets is associated with increased seizures, body weight, and autistic behaviors in neurodevelopmental disability models. 5,34,52 This study provides the first proteomic analysis of potential FXS protein biomarkers in response to specific diets. In this study, state-ofthe-art spatially resolved proteomic MALDI-MS imaging was employed, and LC-ESI MS/MS quantitative proteomics was integrated to systematically evaluate the spatial and dynamic changes of potential protein and peptide markers induced by the consumption of a soy protein-based diet by KO mice. We successfully developed a high-sensitivity and robust strategy to resolve the spatial distribution of protein candidates, which enabled the identification of 1250 mass spectral peaks across the whole brain region of four different cohorts (Figure 1c). To better understand the relationship between aberrant protein spatial distribution and the FXS pathology of soy consumption, MS imaging peaks were further annotated based on the on-tissue peptide extraction results. Nearly 69% of unique peptides from LC-MS/MS could be matched with the MS imaging peak list at a high degree of mass accuracy (<50 ppm); matched peaks displayed excellent reproducibility among biological replicates of all cohorts. Of note, highquality in situ MS/MS imaging results further provided a basis for the credibility of our MALDI-MSI procedure. Thus, the spatially resolved proteomics strategy, guided by MALDI-MSI tryptic-digested peptide imaging, could potentially allow mapping of the global-scale peptide changes in FXS.

To overcome the challenges posed by lower S/N of MALDIproduced precursor ions and limited quantification capacity, we conducted an LC-MS/MS label-free quantitative analysis of proteomes extracted from isolated HPC and HPT brain regions. Overall, we quantified 109 (WT group) and 72 (KO group) proteins in HPT and 206 (WT group) and 245 (KO group) proteins in HPC that were significantly and differentially expressed as a function of Fmr1 genotype or soy protein-based diet. Many candidate proteins played critical roles in the postsynaptic structure and signaling among our list of significantly altered proteins in the KO group in HPT and HPC. Interestingly, most GO terms involved in HPT were also enriched in HPC, clearly showing disparities between the two regions upon exposure to soy consumption. For example, Gpi and ENO1 demonstrated significant changes only in HPC, while APP exhibited significant changes in HPT of the KO group but not in the HPC KO group. These alterations may indicate that varied brain regions differentially respond to the soy diet. It remains to be determined how soy affects FMRP interaction with APP mRNA and contributes to altered translation and/or processing of APP. It should be noted that FXS is not associated with increased neurodegeneration, but altered soluble APP metabolite levels are found in FXS and autism.³⁵ We further connected proteins to genes that are predisposed for AD. Our screen identified 17 significantly altered proteins genetically linked to LOAD, such as cleft lip and palate transmembrane protein 1 (Clptm1), which interacted with all GABAAR subunits.³⁶ The GABAAergic system is involved in the pathophysiology of the fragile X syndrome³⁷ and is also dysregulated in the HPT KO group. These findings indicate that some of the genes linked to LOAD also have altered protein products in the KO mouse brain, further highlighting the intriguing connection between AD and FXS, which warrants future mechanistic investigation. To

arrive at a consensus view of the proteomic changes in HPT and HPC brain regions in response to soy consumption in WT and KO mice, we performed WGCNA analyses and revealed that the protein coexpression families correlated most strongly to the soy diet included synaptic and mitochondrial families. Decreased key glycolytic and TCA cycle enzyme levels, which could explain an abnormal mitochondrial proton leak that impairs synaptic plasticity,³¹ may be regulated by soy consumption. Finally, when comparing shotgun proteomic results with MALDI-MSI data, we found that nearly 86% of MS imaging data were quantified in LC-MS/MS proteomics data sets. IHC staining was performed to validate MS-based studies and was found to be consistent with the MSI results where ENO1 was highly expressed in the KO-S cohort compared to that in KO-C. Of note, previously identified FMRP targets, such as Mapt, Gpi, and Stmn1, showed overlapping spatial distribution and LC-MS/MS quantification results. However, some unique protein candidates were detected with only one strategy, highlighting the complementarity of these two approaches. GAPDH, a key glycolytic enzyme, was upregulated in the soy cohorts when compared to the casein cohorts across the brain regions in the KO group. mGluR5, which is strongly linked to FXS pathology, was downregulated in the KO group in HPC in the LC-MS/MS data set.

To compare our data with the FXS proteomics literature, Klemmer and colleagues 38 identified 23 hippocampal synaptic proteins that differed between WT and KO (C57BL/6J background) mice during early development by quantitative proteomics. We confirmed the presence of all 23 synaptic proteins by global shotgun proteomics in both the WT and KO hippocampus (Table S5).

Of interest, two of these proteins involved in axon sprouting, BASP1 and GAP43, as well as the glycolytic enzyme ENO1 overlapped with our imaging mass spectrometry data set (Table S8, sheet 3). BASP1 and GAP43 were downregulated in the WT hippocampus in response to soy; ENO1 was upregulated in both the hippocampus and hypothalamus in response to soy. Liao and colleagues identified 132 proteins in the primary cortical neurons of WT versus KO mice.³⁹ The only overlap with our mass spectrometry imaging data set was enolase. They identified gamma enolase, also known as ENO2, which was downregulated in the KO group. We identified alpha enolase (ENO1), which was upregulated in the KO hippocampus and hypothalamus in response to soy. Enolase is an important enzyme in glycolysis that catalyzes the conversion of 2-phosphoglycerate to phosphoenolpyruvate, the penultimate step of glycolysis. There is a switch from alpha to gamma enolase in neural tissue during development. Tang and colleagues⁴⁰ examined age-dependent changes in synaptic protein expression in WT versus KO crude synaptoneurosomes (P17 versus P45, FVB strain background). ENO1 and ENO2 were upregulated in the KO at P17 but not P45. Bowling and colleagues⁴¹ identified BASP1, GAP43, and the ENO2 isoform among the top candidates in the KO hippocampus in response to mGluR5 stimulation with DHPG.

Overall, the novel, state-of-the-art, spatially resolved proteomics methodology employed here has a strong probability of identifying potential protein biomarkers in response to genetics, diet, and drug treatment. This procedure may be applied to various diseases to identify diagnostic or prognostic indicators and to further identify targets for therapeutic intervention.

MATERIALS AND METHODS

Mouse Husbandry, Test Diets, and Tissue Collection. WT and KO mice in the C57BL/6J background were bred in our colony maintained at the University of Wisconsin-Madison. Animals were housed in microisolator cages on a 12 h light cycle with ad libitum access to food (Teklad 2019) and water. All husbandry and euthanasia procedures were performed in accordance with National Institutes of Health (NIH) guidelines and an approved University of Wisconsin-Madison Institutional Animal Care and Use Committee (IACUC) protocol administered through the University of Wisconsin Research Animal Resource Center. Breeder Fmr1HET females and WT and Fmr1KO males were transferred to the test diets for at least 12 d prior to breeding. Test diets were formulated and synthesized by Envigo Teklad Diets (Madison, WI) based on their AIN-93G diet (TD.94045). The soy protein-based diet (TD.180375) contained soy protein isolates swapped for casein protein and matched for macronutrient content (protein 18.8% kcal, carbohydrate 64.1% kcal, fat 17.1% kcal; 3.8 kcal/g) and included 0.5% calcium, 0.3% available phosphorus, 0.2% sodium, 0.36% potassium, 0.3% chloride, and 0.05% magnesium. Green food dye was added for visual differentiation. The casein protein-based diet (TD.180374) was a modified version of AIN-93G (TD.94045) with the sodium increased to 0.2% to match the soy diet and red food dye added for visual differentiation (protein 18.9% kcal, carbohydrate 63.8% kcal, fat 17.3% kcal; 3.7 kcal/g). Offspring (WT and Fmr1^{KO} male littermates) were weaned at postnatal day 18 (P18) and maintained on their respective diets until tissue harvest at 3 months. Genotypes were determined by PCR analysis of DNA extracted from tail biopsies taken at weaning. For tissue harvest, mice were anesthetized with isoflurane, perfused with 30 mL of phosphate-buffered saline via the left ventricle, decapitated, and either (1) HPT and HPC brain regions were dissected and the tissue flash was frozen on dry ice and stored at −80 °C or (2) the whole intact brain was removed from the skull, cut in half along the midline with hemispheres immediately placed in disposable base molds, and covered/embedded with melted 10% gelatin. Gelatin molds were stored at -80 °C until processing. 8 μm thick sagittal tissue sections were obtained using a cryostat microtome (HM525, Thermo Fisher Scientific, Waltham, MA). Three consecutive sections from each brain were thaw-mounted onto indium-tinoxide (ITO)-coated glass slides and stored at -80 °C. All sections underwent the tissue digestion procedure, with one section used for MADLI-IMS and two sections used for annotation experiments by LC-MS/MS. For global quantitative proteomic analyses, HPT and HPC were sonicated (3 s on and 3 s off, amplitude 50%) and subjected to enzymatic digestion.

Sample Preparation for MALDI MS Imaging. Endogenous background compounds (lipids and peptides) were removed using original washing or Carnoy's washing methods.⁴² In the original method, tissues were washed twice in 70% ethanol for 30 s and in 100% ethanol for 30 s. In Carnoy's method, tissues were washed as follows: they were submerged in (i) 70% ethanol for 30 s; (ii) 100% ethanol for 30 s; (iii) Carnoy's buffer (ethanol/chloroform/acetic acid 6:3:1) for 2 min; (iv) 100% ethanol for 30 s; (v) optima grade water for 30 s; and (vi) 100% ethanol for 30 s. The sections were then allowed to dry for 15 min under vacuum. Enzyme and matrix applications were performed by a robotic TM sprayer system (HTX Technologies, Carrobo, NC). For enzyme deposition, trypsin was dissolved in 15 mM ammonium bicarbonate to a final concentration of 0.05 μ g/ μ L and sprayed at a flow rate of 0.02 mL/min with a total of 8 passes performed. The nozzle temperature was set to 30 $^{\circ}\text{C}$ with a moving velocity of 750 mm/min. Then, tissue sections were incubated in a humidity chamber at 37 °C for 4 h. α-Cyano-4hydroxycinnamic acid (CHCA) dissolved in 70% acetonitrile (ACN) and 1% trifluoroacetic acid (TFA) solution at a concentration of 10 mg/mL was used as the matrix for peptide imaging. A total of 4 passes of matrix spraying were performed at a flow rate of 0.12 mL/min and a 30 s drying time between each pass. The nozzle temperature was set to 75 °C with a moving velocity of 800 mm/min. The slides were

dried in a desiccator at room temperature for 15 min and subjected to an instrument analysis.

MALDI MS Imaging. MALDI-MS imaging was performed on a Bruker RapifleX MALDI Tissuetyper TOF/TOF (Bruker, Billerica, MA) equipped with a smart-beam 3D 10 kHz laser. Samples were analyzed in positive-ion mode with an m/z range of 600 to 3000, 80% laser energy, and a 50 μ m step size.

Peptide Extraction. Consecutive tissue sections were prepared for MALDI-MSI using the same sample preparation protocol as above. After trypsin deposition, the proteolytic peptides were extracted from the ITO slides using the following protocol: (i) 40 μ L of 0.1% TFA (repeat 4 times); (ii) 40 μ L of 50% ACN, 0.1% TFA (repeat 4 times); and (iii) 90% ACN, 0.1% TFA (repeat 4 times). Four extracts from each brain were combined, dried, resuspended in 0.1% TFA, and then cleaned with an Omix C18 tip (Agilent). The purified extracts were dried and stored at -20 °C until LC-ESI-MS/MS analysis.

Sample Preparation for Global Proteomic Analysis. HPT and HPC tissues were homogenized in lysis buffer (8 M urea, 50 mM tris) using a probe sonicator, and protein concentration was determined using a BCA protein assay kit (Thermo Pierce, Rockford, IL) as per the manufacturer's instructions. Samples were reduced with 100 mM DTT for 1 h and alkylated with 200 mM IAA for 30 min before quenching with 100 mM DTT. Proteins were digested by trypsin at 37 °C for 16 h in a 50:1 (protein/enzyme) ratio. Digests were quenched by lowering the pH to <3 with 10% TFA. Peptides were desalted with SepPak C18 solid-phase extraction (SPE) cartridges (Waters, Milford, MA). All samples were dried in vacuo and stored at -80 °C until LC-ESI-MS/MS analysis.

LC–MS/MS Acquisition. Samples from imaging peptide extraction were dissolved in 0.1% FA and analyzed on the Orbitrap Fusion LumosTM Tribrid mass spectrometer (Thermo Fisher Scientific, Bremen, Germany) coupled to a Dionex UPLC system. Samples' global proteomic analysis was analyzed on the Orbitrap Q-Exactive HF mass spectrometer (Thermo Fisher Scientific, Bremen, Germany). The chromatographic separation was carried out via a mobile phase A that consists of 0.1% FA in water and a mobile phase B consisting of 0.1% FA in ACN. Peptides were loaded onto a 75 μ m \times 15 cm homemade column packed with 1.7 μ m, 130 Å, BEH C18 material obtained from a Waters UPLC column (part no. 186004661). Emitter tips were pulled from 75 μ m i.d. capillary tubing (Polymicro Technologies, Phoenix, AZ) using a model P-2000 laser puller (Sutter Instrument Co., Novato, CA).

For imaging peptide extracts, the LC gradient was set as follows: 5-8% B (18-30 min), 8-22% B (30-100 min), and 22-40% B (100-120 min) with a flow rate of 300 nL/min. Survey scans of peptide precursors were performed with a scan range from 300 to 1500 m/z at a resolving power of 60 K (at m/z 200) with an automatic gain control (AGC) target of 2×10^6 and a maximum injection time of 100 ms. The top 20 precursors were then selected for higher-energy C-trap dissociation tandem mass spectrometry (HCD MS²) analysis with an isolation width of 1 Da, a normalized collision energy (NCE) of 30, a resolving power of 15 K (at m/z 200), an AGC target of 1×10^4 , a maximum injection time of 100 ms, and a lower mass limit of 120 m/z. Precursors were subjected to dynamic exclusion for 45 s with a 10 ppm tolerance. Each sample was acquired in a technical triplicate.

For global proteomic samples, the LC gradient was set as follows: $3{\text -}10\%$ B ($18{\text -}31$ min), $10{\text -}24\%$ B ($31{\text -}95$ min), and $24{\text -}35\%$ B ($95{\text -}127$ min) with a flow rate of 300 nL/min. Survey scans of peptide precursors were performed with a scan range from 300 to 2000 m/z at a resolving power of 60 K (at m/z 200) with an AGC target of 1×10^6 and a maximum injection time of 100 ms. The top 15 precursors were then selected for HCD MS² analysis with an isolation width of 2 Da, a NCE of 28, a resolving power of 15 K (at m/z 200), an AGC target of 2×10^5 , a maximum injection time of 150 ms, and a lower mass limit of 100 m/z. Precursors were subject to dynamic exclusion for 18 s with a 10 ppm tolerance. Each sample was acquired in technical triplicate.

Data Analysis. For MALDI MS imaging data analysis, ROIs were selected in flexImaging (Bruker, Billerica, MA) and imported into SCiLS Lab for spectra smoothed alignment ¹⁶ and total ion intensity (TIC) normalization. Overview spectra were then exported for peak picking to mMass, and peptide annotation was performed by matching tissue-specific peaks with on-tissue peptide extraction results from LC-MS/MS. The detected peaks were reimported into the SCiLS Lab for subsequent segmentation and statistical analysis. *t*-SNE clustering was accomplished using a Python implementation of the *t*-distributed stochastic neighbor embedding algorithm, which is made available through the machine learning library, scikit learn. Iterative optimization was performed to establish the most appropriate parameters.

Protein identification and quantification was done by MaxQuant (version 1.5.3.8)-based database searching using the integrated Andromeda search engine with a FDR < 1% at peptide and protein levels. The tandem mass spectra were searched against the Mus musculus UniProt database (version updated December 2018). A reverse database for the decoy search was generated automatically in MaxQuant. Enzyme specificity was set to "trypsin/p", and a minimum number of seven amino acids were required for peptide identification. For label-free protein quantification (LFQ), the MaxQuant LFQ algorithm was used to quantitate the MS signals, and the proteins' intensities were represented in LFQintesnity. 43 Cysteine carbamidomethylation was set as the fixed modification. The oxidation of M and the acetylation of the protein N-terminus were set as the variable modifications. The first search mass tolerance was 20 ppm, and the main search peptide tolerance was 4.5 ppm. The false discovery rates of the peptide-spectrum matches and proteins were set to less than 1%. For peptide quantification, the intensities of all samples were extracted from the MaxQuant result peptide files. Then, the expression matrix was subjected to normalization followed by log₂transformation by Perseus.44 From three technical replicates, the mean protein intensities were calculated for each biological replicate and subjected to a statistical analysis. Bioinformatic analyses were performed with an R software environment. GO analyses were generated using Metascape²⁷ (version 3.5) and DAVID bioinformatics resources 45 with a FDR cutoff of 0.05. The WGCNA algorithm was used for network analysis as previously described. 46

Immunohistochemistry Staining. Immunohistochemical (IHC) procedures were performed as previously described.⁴⁷ For mouse IHC, all brain slices (8 μ m) were processed exactly the same for comparison. Consecutive tissue slices were fixed with 4% paraformaldehyde (PFA) for 45 min. Tissue slices were washed three times in TBS and blocked in 5% goat serum and 2% BSA plus 0.5% Triton X-100. After blocking for 1 h at room temperature (RT), slices were incubated with avidin and biotin for 15 min successively for membrane permeabilization. Then, the slices were incubated with polyclonal anti-ENO1 (Thermo Fisher, PA5-21387, 1:500) and the isotype- and concentration-matched normal IgG control (ab172730, Abcam, Cambridge, MA) in an antibody dilution buffer (Cell Signaling Technology, 12378S) overnight at 4 $^{\circ}\text{C}.$ After three washes in TBST, 6 min each, the slides were incubated for 15 min with goat antirabbit secondary antibodies (Thermo Fisher, 5082867). After three washes with TBST, 6 min each, the slides were incubated with the HRP solution (Biocare Medical, PX968M) for 15 min and counter-stained with a 1:30 dilution of DAB-chromogen (Thermo Fisher, 5082374) and hematoxylin (Sigma, HHS16). Mouse brain slice images were taken with a Leica microscope (Leica, DM5000), a bright field camera, and a 20× objective. The IHC intensities of proteins were determined by ImageJ software with an IHC profiler plugin.⁴⁸ Images were acquired with the same setting for all slides. Images were acquired for each HPC mouse brain ROI, and in every image, measures were averaged to give the value for each animal. Each cohort had three biological replicates.

ASSOCIATED CONTENT

Data Availability Statement

The mass spectrometry data have been deposited to the ProteomeXchange Consortium⁴⁹ via the PRIDE⁵⁰ partner repository with the data set identifier PXD034326. Public release of the data will be made in time for the online publication of the paper.

Supporting Information

The Supporting Information is available free of charge at https://pubs.acs.org/doi/10.1021/acschemneuro.3c00497.

t-SNE analysis method; MALDI-MSI data reproducibility; illustrative in situ MALDI-TOF/TOF spectrum; data correlation with the public database; exemplification of the t-SNE analysis; comprehensive proteomic analysis of mouse HPT and HPC; WGCNA coexpression network exploration and GO analysis; and spatially resolved markers for shotgun proteomic analysis compatibility (PDF)

Gelatin trypsin digestion peaks (XLSX)

KEGG pathway of 341 proteins (XLSX)

Specific uniquely modified peptides in each cohort (XLSX)

Identification and quantification of proteins in the hypothalamus (XLSX)

Quantification results of the *Fmr1* KO group (XLSX) Specific changed proteins in WT and KO in the hypothalamus (XLSX)

Proteins changed only in the *Fmr1* KO group (XLSX) Protein overlap between MALDI MSI and significantly changed proteomics data (XLSX)

AUTHOR INFORMATION

Corresponding Authors

Cara J. Westmark — Department of Neurology and Molecular Environmental Toxicology Center, School of Medicine and Public Health, University of Wisconsin-Madison, Madison, Wisconsin 53706, United States; Email: westmark@ wisc.edu

Lingjun Li — School of Pharmacy, University of Wisconsin-Madison, Madison, Wisconsin 53705, United States; Department of Chemistry, Lachman Institute for Pharmaceutical Development, School of Pharmacy, and Wisconsin Center for NanoBioSystems, School of Pharmacy, University of Wisconsin-Madison, Madison, Wisconsin 53705, United States; orcid.org/0000-0003-0056-3869; Email: lingjun.li@wisc.edu

Authors

Min Ma – School of Pharmacy, University of Wisconsin-Madison, Madison, Wisconsin 53705, United States

Qinying Yu — School of Pharmacy, University of Wisconsin-Madison, Madison, Wisconsin 53705, United States

Daniel G. Delafield — School of Pharmacy, University of Wisconsin-Madison, Madison, Wisconsin 53705, United States; © orcid.org/0000-0003-2989-9833

Yusi Cui — Department of Chemistry, University of Wisconsin-Madison, Madison, Wisconsin 53705, United States

Zihui Li – Department of Chemistry, University of Wisconsin-Madison, Madison, Wisconsin 53705, United States

Miyang Li – Department of Chemistry, University of Wisconsin-Madison, Madison, Wisconsin 53705, United States

Wenxin Wu – Department of Chemistry, University of Wisconsin-Madison, Madison, Wisconsin 53705, United States

Xudong Shi – Division of Otolaryngology, Department of Surgery, University of Wisconsin-Madison, Madison, Wisconsin 53705, United States

Pamela R. Westmark – Department of Neurology, University of Wisconsin-Madison, Madison, Wisconsin 53706, United States

Alejandra Gutierrez – Department of Neurology and Molecular Environmental Toxicology Center, School of Medicine and Public Health, University of Wisconsin-Madison, Madison, Wisconsin 53706, United States

Gui Ma – McArdle Laboratory for Cancer Research, University of Wisconsin-Madison, Madison, Wisconsin 53705, United States

Ang Gao — McArdle Laboratory for Cancer Research, University of Wisconsin-Madison, Madison, Wisconsin 53705, United States

Meng Xu – Department of Chemistry, University of Wisconsin-Madison, Madison, Wisconsin 53705, United States

Wei Xu – McArdle Laboratory for Cancer Research, University of Wisconsin-Madison, Madison, Wisconsin 53705, United States

Complete contact information is available at: https://pubs.acs.org/10.1021/acschemneuro.3c00497

Author Contributions

OM.M. and Q.Y. contributed equally to this work. M.M., Q.Y., C.W., and L.L. designed the study and conceived the experiments. M.M. and Q.Y. conducted the experiments, analyzed the data, and wrote the first draft of the manuscript; G.D., Y.C., Z.L., M.L., W.W., and M.X. assisted with data analysis and organization and some figure making; X.S. performed the H&E staining; G.M., A.G., and W.X. performed the IHC staining; and A.G. and P.W. bred and treated mice, collected tissue samples, and prepared gelatin-embedded tissues. M.M., Q.Y., C.W., and L.L. prepared and revised the manuscript, and all authors provided editorial feedback and input.

Notes

The authors declare no competing financial interest.

■ ACKNOWLEDGMENTS

This work was supported in part by the United States Department of Agriculture (grant number 2018-67001-28266 to C.W. and L.L.) and the University of Wisconsin Pandemic-Affected Research Continuation Initiative (PARCI). L.L. would like to acknowledge NIH grants R01 AG078794, R01DK071801, R56MH110215, and R01AG052324; NCRR grants S10RR029531, S10OD025084, and S10 OD028473; and NSF grant IOS-2010789, as well as a Vilas Distinguished Achievement Professorship and a Charles Melbourne Johnson Professorship with funding provided by the Wisconsin Alumni Research Foundation and the University of Wisconsin-Madison School of Pharmacy. M.X. would like to acknowledge the National Science Foundation Graduate Research Fellowship Program under grant no. DGE-1747503. The funding bodies played no role in study design; the collection, analysis, and interpretation of data; manuscript preparation; or the decision to publish.

ABBREVIATIONS

FXS, fragile X syndrome; FMRP, fragile X messenger ribonucleoprotein; HPC, hippocampus; HPT, hypothalamus; WT-C, wild-type casein group; WT-S, wild-type soy group; KO-C, Fmr1KO casein group; KO-S, Fmr1KO soy group; MBP, myelin basic protein; NEFM, neurofilament medium polypeptide; LC-MS/MS, liquid chromatography-tandem mass spectrometry; MALDI, matrix-assisted laser desorption/ ionization; Aco2, aconitate hydratase; Ckb, creatine kinase Btype; Ncam1, neural cell adhesion molecule 1; Hnrnpa2b1, heterogeneous nuclear ribonucleoprotein A2/B1; ASDs, autism spectrum disorders; Atp1b1, sodium/potassium-transporting ATPase subunit β -1; Crmp1, dihydropyrimidinaserelated protein 1; Arhgef2, rho guanine nucleotide exchange factor 2; APP, amyloid- β precursor protein; HPCAL1, hippocalcin-like protein 1; ENO1, glycolytic enzyme enolase 1; GAPDH, glyceraldehyde-3-phosphate dehydrogenase; STMN1, stathmin; GPI, glucose-6-phosphate isomerase; MAPT, microtubule-associated protein tau; mGluR5, glutamate receptor 5; FDR, false discovery rate; WGCNA, weighted correlation network analysis; M, module; ME, module eigenproteins; GO, Gene Ontology; KEGG, Kyoto Encyclopedia of Genes and Genomes

REFERENCES

- (1) Brown, V.; Jin, P.; Ceman, S.; Darnell, J. C.; O'Donnell, W. T.; Tenenbaum, S. A.; Jin, X.; Feng, Y.; Wilkinson, K. D.; Keene, J. D.; et al. Microarray identification of FMRP-associated brain mRNAs and altered mRNA translational profiles in fragile X syndrome. *Cell* **2001**, 107 (4), 477–487.
- (2) Westmark, C. J.; Westmark, P. R.; Malter, J. S. Soy-based diet exacerbates seizures in mouse models of neurological disease. *J. Alzheimer's Dis.* **2013**, 33 (3), 797–805.
- (3) Alam, S.; Westmark, C. J.; McCullagh, E. A. Diet in treatment of autism spectrum disorders. *Front. Neurosci.* **2023**, *16*, 1031016.
- (4) Westmark, C. J. Soy-Based Therapeutic Baby Formulas: Testable Hypotheses Regarding the Pros and Cons. Front. Nutr. 2017, 3, 59.
- (5) Westmark, C. J.; Kniss, C.; Sampene, E.; Wang, A.; Milunovich, A.; Elver, K.; Hessl, D.; Talboy, A.; Picker, J.; Haas-Givler, B.; et al. Soy-Based Infant Formula is Associated with an Increased Prevalence of Comorbidities in Fragile X Syndrome. *Nutrients* **2020**, *12* (10), 3136
- (6) Guo, L.; Lai, Z.; Wang, Y.; Li, Z. In situ probing changes in fatty-acyl chain length and desaturation of lipids in cancerous areas using mass spectrometry imaging. *J. Mass Spectrom.* **2020**, *56* (4), No. e4621.
- (7) Seeley, E. H.; Liu, Z.; Yuan, S.; Stroope, C.; Cockerham, E. D.; Rashdan, N.; Finney, A. C.; Kumar, D.; Das, S.; Razani, B. Spatially Resolved Metabolites in Stable and Vulnerable Human Atherosclerotic Plaques Identified by Mass Spectrometry Imaging. *Arterioscler., Thromb., Vasc. Biol.* 2023, 43, 1626.
- (8) Li, H.; Hummon, A. B. Imaging mass spectrometry of three-dimensional cell culture systems. *Anal. Chem.* **2011**, 83 (22), 8794–8801.
- (9) Casadonte, R.; Caprioli, R. M. Proteomic analysis of formalin-fixed paraffin-embedded tissue by MALDI imaging mass spectrometry. *Nat. Protoc.* **2011**, *6* (11), 1695–1709.
- (10) Malaker, S. A.; Quanico, J.; Raffo-Romero, A.; Kobeissy, F.; Aboulouard, S.; Tierny, D.; Bertozzi, C. R.; Fournier, I.; Salzet, M. On-tissue spatially resolved glycoproteomics guided by N-glycan imaging reveal global dysregulation of canine glioma glycoproteomic landscape. *Cell Chem. Biol.* **2022**, *29*, 30–42.e4.
- (11) Shariatgorji, M.; Nilsson, A.; Fridjonsdottir, E.; Vallianatou, T.; Kallback, P.; Katan, L.; Savmarker, J.; Mantas, I.; Zhang, X.; Bezard, E.; et al. Comprehensive mapping of neurotransmitter networks by MALDI-MS imaging. *Nat. Methods* **2019**, *16*, 1021–1028.

- (12) Groseclose, M. R.; Castellino, S. A mimetic tissue model for the quantification of drug distributions by MALDI imaging mass spectrometry. *Anal. Chem.* **2013**, *85* (21), 10099–10106.
- (13) Chughtai, K.; Heeren, R. M. Mass spectrometric imaging for biomedical tissue analysis. *Chem. Rev.* **2010**, *110* (5), 3237–3277.
- (14) DeLaney, K.; Phetsanthad, A.; Li, L. Advances in high-resolution maldi mass spectrometry for neurobiology. *Mass Spectrom. Rev.* **2022**, *41* (2), 194–214.
- (15) Yang, J.; Caprioli, R. M. Matrix sublimation/recrystallization for imaging proteins by mass spectrometry at high spatial resolution. *Anal. Chem.* **2011**, *83* (14), 5728–5734.
- (16) Boskamp, T.; Lachmund, D.; Casadonte, R.; Hauberg-Lotte, L.; Kobarg, J. H.; Kriegsmann, J.; Maass, P. Using the Chemical Noise Background in MALDI Mass Spectrometry Imaging for Mass Alignment and Calibration. *Anal. Chem.* **2020**, 92 (1), 1301–1308.
- (17) Guo, G.; Papanicolaou, M.; Demarais, N. J.; Wang, Z.; Schey, K. L.; Timpson, P.; Cox, T. R.; Grey, A. C. Automated annotation and visualisation of high-resolution spatial proteomic mass spectrometry imaging data using HIT-MAP. *Nat. Commun.* **2021**, *12* (1), 3241.
- (18) Alarcon, C. R.; Goodarzi, H.; Lee, H.; Liu, X.; Tavazoie, S.; Tavazoie, S. F. HNRNPA2B1 Is a Mediator of m(6)A-Dependent Nuclear RNA Processing Events. *Cell* **2015**, *162* (6), 1299–1308.
- (19) Croning, M. D.; Marshall, M. C.; McLaren, P.; Armstrong, J. D.; Grant, S. G. G2Cdb: the Genes to Cognition database. *Nucleic Acids Res.* **2009**, *37*, D846–D851.
- (20) Cao, G.; Li, K.; Guo, J.; Lu, M.; Hong, Y.; Cai, Z. Mass Spectrometry for Analysis of Changes during Food Storage and Processing. *J. Agric. Food Chem.* **2020**, *68* (26), *6956–6966*.
- (21) Timper, K.; Bruning, J. C. Hypothalamic circuits regulating appetite and energy homeostasis: pathways to obesity. *Dis. Models Mech.* **2017**, *10* (6), 679–689.
- (22) Kanoski, S. E.; Grill, H. J. Hippocampus Contributions to Food Intake Control: Mnemonic, Neuroanatomical, and Endocrine Mechanisms. *Biol. Psychiatry* **2017**, *81* (9), 748–756.
- (23) Darnell, J. C.; Van Driesche, S.; Zhang, C.; Hung, K. Y.; Mele, A.; Fraser, C. E.; Stone, E. F.; Chen, C.; Fak, J. J.; Chi, S. W.; et al. FMRP stalls ribosomal translocation on mRNAs linked to synaptic function and autism. *Cell* **2011**, *146* (2), 247–261.
- (24) Basu, S. N.; Kollu, R.; Banerjee-Basu, S. AutDB: a gene reference resource for autism research. *Nucleic Acids Res.* **2009**, *37* (suppl_1), D832–D836.
- (25) Li, Z.; Zhang, Y.; Ku, L.; Wilkinson, K. D.; Warren, S. T.; Feng, Y. The fragile X mental retardation protein inhibits translation via interacting with mRNA. *Nucleic Acids Res.* **2001**, 29 (11), 2276–2283.
- (26) Pacey, L. K.; Xuan, I. C.; Guan, S.; Sussman, D.; Henkelman, R. M.; Chen, Y.; Thomsen, C.; Hampson, D. Delayed myelination in a mouse model of fragile X syndrome. *Hum. Mol. Genet.* **2013**, 22 (19), 3920–3930.
- (27) Zhou, Y.; Zhou, B.; Pache, L.; Chang, M.; Khodabakhshi, A. H.; Tanaseichuk, O.; Benner, C.; Chanda, S. K. Metascape provides a biologist-oriented resource for the analysis of systems-level datasets. *Nat. Commun.* **2019**, *10* (1), 1523.
- (28) Westmark, C. J.; Malter, J. S. FMRP mediates mGluR5-dependent translation of amyloid precursor protein. *PLoS Biol.* **2007**, 5 (3), No. e52.
- (29) Bertram, L.; McQueen, M. B.; Mullin, K.; Blacker, D.; Tanzi, R. E. Systematic meta-analyses of Alzheimer disease genetic association studies: the AlzGene database. *Nat. Genet.* **2007**, *39* (1), 17–23.
- (30) Zhang, D.; Liu, X.; Xu, X.; Xu, J.; Yi, Z.; Shan, B.; Liu, B. HPCAL 1 promotes glioblastoma proliferation via activation of Wnt/ β -catenin signalling pathway. *J. Cell. Mol. Med.* **2019**, 23 (5), 3108–3117.
- (31) Licznerski, P.; Park, H. A.; Rolyan, H.; Chen, R.; Mnatsakanyan, N.; Miranda, P.; Graham, M.; Wu, J.; Cruz-Reyes, N.; Mehta, N.; et al. ATP Synthase c-Subunit Leak Causes Aberrant Cellular Metabolism in Fragile X Syndrome. *Cell* **2020**, *182* (5), 1170–1185.e9.

- (32) Cumming, R. C.; Schubert, D. Amyloid-beta induces disulfide bonding and aggregation of GAPDH in Alzheimer's disease. *FASEB J.* **2005**, *19* (14), 2060–2062.
- (33) Bear, M. F.; Huber, K. M.; Warren, S. T. The mGluR theory of fragile X mental retardation. *Trends Neurosci.* **2004**, *27* (7), 370–377.
- (34) Westmark, C. J. Soy Infant Formula may be Associated with Autistic Behaviors. *Autism: Open Access* 2013, 3, 20727.
- (35) Westmark, C. J.; Sokol, D. K.; Maloney, B.; Lahiri, D. K. Novel roles of amyloid-beta precursor protein metabolites in fragile X syndrome and autism. *Mol. Psychiatry* **2016**, *21* (10), 1333–1341.
- (36) Ge, Y.; Kang, Y.; Cassidy, R. M.; Moon, K.-M.; Lewis, R.; Wong, R. O.; Foster, L. J.; Craig, A. M. Clptm1 limits forward trafficking of GABAA receptors to scale inhibitory synaptic strength. *Neuron* **2018**, *97* (3), 596.
- (37) Yang, Y.-M.; Arsenault, J.; Bah, A.; Krzeminski, M.; Fekete, A.; Chao, O. Y.; Pacey, L. K.; Wang, A.; Forman-Kay, J.; Hampson, D. R. Identification of a molecular locus for normalizing dysregulated GABA release from interneurons in the Fragile X brain. *Mol. Psychiatry* **2020**, 25 (9), 2017–2035.
- (38) Klemmer, P.; Meredith, R. M.; Holmgren, C. D.; Klychnikov, O. I.; Stahl-Zeng, J.; Loos, M.; van der Schors, R. C.; Wortel, J.; de Wit, H.; Spijker, S.; et al. Proteomics, ultrastructure, and physiology of hippocampal synapses in a fragile X syndrome mouse model reveal presynaptic phenotype. *J. Biol. Chem.* **2011**, 286 (29), 25495–25504.
- (39) Liao, L.; Park, S. K.; Xu, T.; Vanderklish, P.; Yates, J. R. J. P. o. t. N. A. o. S. Quantitative proteomic analysis of primary neurons reveals diverse changes in synaptic protein content in fmr1 knockout mice. *Proc. Natl. Acad. Sci. U.S.A.* **2008**, *105* (40), 15281–15286.
- (40) Tang, B.; Wang, T.; Wan, H.; Han, L.; Qin, X.; Zhang, Y.; Wang, J.; Yu, C.; Berton, F.; Francesconi, W.; et al. Fmr1 deficiency promotes age-dependent alterations in the cortical synaptic proteome. *Proc. Natl. Acad. Sci. U.S.A.* **2015**, *112* (34), No. E4697.
- (41) Bowling, H.; Bhattacharya, A.; Zhang, G.; Alam, D.; Lebowitz, J. Z.; Bohm-Levine, N.; Lin, D.; Singha, P.; Mamcarz, M.; Puckett, R.; et al. Altered steady state and activity-dependent de novo protein expression in fragile X syndrome. *Nat. Commun.* **2019**, *10* (1), 1710.
- (42) Deutskens, F.; Yang, J.; Caprioli, R. M. High spatial resolution imaging mass spectrometry and classical histology on a single tissue section. *J. Mass Spectrom.* **2011**, *46* (6), 568–571.
- (43) Schaab, C.; Geiger, T.; Stoehr, G.; Cox, J.; Mann, M. Analysis of high accuracy, quantitative proteomics data in the MaxQB database. *Mol. Cell. Proteomics* **2012**, *11* (3), M111 014068.
- (44) Tyanova, S.; Temu, T.; Sinitcyn, P.; Carlson, A.; Hein, M. Y.; Geiger, T.; Mann, M.; Cox, J. The Perseus computational platform for comprehensive analysis of (prote)omics data. *Nat. Methods* **2016**, *13* (9), 731–740.
- (45) Huang, D. W.; Sherman, B. T.; Lempicki, R. A. Systematic and integrative analysis of large gene lists using DAVID bioinformatics resources. *Nat. Protoc.* **2009**, *4* (1), 44–57.
- (46) McKenzie, A. T.; Moyon, S.; Wang, M.; Katsyv, I.; Song, W. M.; Zhou, X.; Dammer, E. B.; Duong, D. M.; Aaker, J.; Zhao, Y.; et al. Multiscale network modeling of oligodendrocytes reveals molecular components of myelin dysregulation in Alzheimer's disease. *Mol. Neurodegener.* 2017, 12 (1), 82.
- (47) Liu, F.; Ma, M.; Gao, A.; Ma, F.; Ma, G.; Liu, P.; Jia, C.; Wang, Y.; Donahue, K.; Zhang, S.; et al. PKM2-TMEM33 axis regulates lipid homeostasis in cancer cells by controlling SCAP stability. *EMBO J.* **2021**, *40* (22), No. e108065.
- (48) Varghese, F.; Bukhari, A. B.; Malhotra, R.; De, A. IHC Profiler: an open source plugin for the quantitative evaluation and automated scoring of immunohistochemistry images of human tissue samples. *PLoS One* **2014**, *9* (5), No. e96801.
- (49) Deutsch, E. W.; Bandeira, N.; Sharma, V.; Perez-Riverol, Y.; Carver, J. J.; Kundu, D. J.; Garcia-Seisdedos, D.; Jarnuczak, A. F.; Hewapathirana, S.; Pullman, B. S.; et al. The ProteomeXchange consortium in 2020: enabling big data approaches in proteomics. *Nucleic Acids Res.* **2019**, *48* (D1), D1145–D1152.
- (50) Perez-Riverol, Y.; Csordas, A.; Bai, J.; Bernal-Llinares, M.; Hewapathirana, S.; Kundu, D. J.; Inuganti, A.; Griss, J.; Mayer, G.;

- Eisenacher, M.; et al. The PRIDE database and related tools and resources in 2019: improving support for quantification data. *Nucleic Acids Res.* **2019**, *47* (D1), D442–D450.
- (51) Westmark, C. J. Fragile X and APP: a decade in review, a vision for the future. *Mol. Neurobiol.* **2019**, *56* (6), 3904–3921.
- (52) Westmark, C. J.; Filon, M. J.; Maina, P.; Steinberg, L. I.; Ikonomidou, C.; Westmark, P. R. Effects of soy-based infant formula on weight gain and neurodevelopment in an autism mouse model. *Cells* **2022**, *11* (8), 1350.